A Preferred Amplitude of Calcium Sparks in Skeletal Muscle

E. Ríos,* N. Shirokova,* W. G. Kirsch,* G. Pizarro,† M. D. Stern,‡ H. Cheng,‡ and A. González*

*Department of Molecular Biophysics and Physiology, Rush University, 1750 W. Harrison Street, Suite 1279 JS, Chicago, Illinois 60612 USA; †Departamento de Biofísica, Facultad de Medicina and Facultad de Ciencias, Montevideo, Uruguay; and ‡Laboratory of Cardiovascular Science, Gerontology Research Center, National Institute of Aging, National Institutes of Health, Baltimore, Maryland 21224 USA

ABSTRACT In skeletal and cardiac muscle, calcium release from the sarcoplasmic reticulum, leading to contraction, often results in calcium sparks. Because sparks are recorded by confocal microscopy in line-scanning mode, their measured amplitude depends on their true amplitude and the position of the spark relative to the scanned line. We present a method to derive from measured amplitude histograms the actual distribution of spark amplitudes. The method worked well when tested on simulated distributions of experimental sparks. Applied to massive numbers of sparks imaged in frog skeletal muscle under voltage clamp in reference conditions, the method yielded either a decaying amplitude distribution (6 cells) or one with a central mode (5 cells). Caffeine at 0.5 or 1 mM reversibly enhanced this mode (5 cells) or induced its appearance (4 cells). The occurrence of a mode in the amplitude distribution was highly correlated with the presence of a mode in the distribution of spark rise times or in the joint distribution of rise times and spatial widths. If sparks were produced by individual Markovian release channels evolving reversibly, they should not have a preferred rise time or amplitude. Channel groups, instead, could cooperate allosterically or through their calcium sensitivity, and give rise to a stereotyped amplitude in their collective spark.

INTRODUCTION

In muscle, action potentials cause intracellular Ca^{2+} channels (ryanodine receptors) to open, and the ensuing Ca^{2+} release initiates contraction. A large fraction of this release occurs by superposition of brief local events, which under fluorescence monitoring appear as Ca^{2+} sparks (Cheng et al., 1993) in cardiac (López-López et al., 1995), skeletal (Tsugorka et al., 1995; Klein et al., 1996), and smooth muscle (Nelson et al., 1995). The mechanism by which sparks are generated is debatable. They are known to involve the phenomenon of Ca^{2+}-induced Ca release (CICR; Endo et al., 1970; Klein et al., 1996; Shirokova and Ríos, 1997) but in skeletal muscle they should ultimately be under membrane voltage control. How voltage and Ca^{2+} interact for the activation of sparks is not known. Even less is known about the process that terminates sparks, which was characterized in cardiac muscle as an inactivation (Sham et al., 1998), and in skeletal muscle appears to be extraordinarily effective, as it terminates the sparks abruptly (Lacampagne et al., 1999) after a stereotyped time interval of a few milliseconds (González et al., 2000b).

To clarify their mechanism, it is important to evaluate the number of release channels involved in individual sparks (reviewed by Schneider, 1999; Cannell and Soeller, 1999; Shirokova et al., 1999). In this regard, knowledge of the spark amplitude appears essential, as it should depend simply on the number of channels involved. Thus, if sparks were produced by single channels, the distribution of amplitudes should depend directly on that of open times. This distribution, in turn, should be monotonically decreasing if the gating of ryanodine receptors was a homogeneous Markov process, as it is for the vast majority of channels (Colquhoun and Hawkes, 1995). Knowledge of spark amplitudes should additionally help answer other fundamental questions about mechanism.

There are obstacles to the evaluation of spark amplitude. Because sparks are imaged by line scanning, and those originating farther from the scanned line appear to have less intensity, the reported amplitude depends as much on the true amplitude of the spark (the height of the fluorescent object) as on its placement relative to the scanned line.

Using a discrete model of the array of release channels, Pratusevich and Balke (1996) predicted that the histogram of detected amplitudes would not have a mode even if all spark objects were identical. Cheng et al. (1999) generalized a treatment of Shirokova and Ríos (1997) to demonstrate theoretically the monotonic character of the distribution, and confirmed it experimentally for both cardiac and skeletal muscle. These contributions showed that the experimental amplitude histogram is far removed from the true distribution of spark amplitudes. In particular, any mode in the true distribution of amplitudes is lost due to the limitations of line scanning.

Bridge et al. (1999) determined the distribution of amplitudes for sparks originated at repetitive firing units, thus eliminating the variability introduced by the distance to the scanning light beam, and found this distribution to have a

Received for publication 30 May 2000 and in final form 12 October 2000.

Dr. Kirsch's present address: Univ. Heidelberg, II Physiologisches Institute, D-69120 Heidelberg. Germany.

Dr. Shirokova's present address: Dept. Pharmacology and Physiology, UMDNJ, Newark, NJ 07103.

Address reprint requests to E. Ríos, Department of Molecular Biophysics and Physiology, Rush University, 1750 W. Harrison Street, Suite 1279 JS, Chicago, IL 60612. Tel.: 312-942-2081; Fax: 312-942-8711; E-mail: erios@rush.edu.

© 2001 by the Biophysical Society

0006-3495/01/01/169/15 $2.00

mode. Although this result weighs in favor of the involvement of multiple channels, it does not help interpret the usual amplitude histograms of events originated at variable, essentially random locations.

Izu et al. (1998) and Cheng et al. (1999) demonstrated under different hypotheses that sets of identical sparks give rise to a distribution of measured amplitudes of simple mathematical form.

Building on this advance, we present here a method for deriving the true distribution of spark amplitudes from that of measured amplitudes. This correction algorithm is then applied to experimental histograms derived from fluorescence images of frog skeletal muscle fibers under voltage clamp. The results are of special interest when the events exhibit a mode in their distribution of rise times, as is the case in the presence of caffeine (González et al., 2000a,b), corresponding to a stereotyped duration of the underlying release channel open times.

METHODS

Experiments were carried out in cut skeletal muscle fibers from *Rana pipiens* semitendinosus muscle, voltage clamped in a two-Vaseline gap chamber on the stage of an inverted microscope. Adult frogs were anaesthetized in 15% ethanol, then killed by pithing. Fibers dissected and mounted as described by González et al. (2000a) were moderately stretched at sarcomere lengths of 3.2 to 3.6 μm.

The "external" solution contained 10 mM $Ca(CH_3SO_3)_2$, 110 mM TEA-CH_3SO_3, 10 mM HEPES, 1 μM tetrodotoxin, and 1 mM 3,4 diaminopyridine. The "internal" solution contained 110 mM cesium glutamate, 1 mM EGTA, 5 mM glucose, 5 mM magnesium ATP, 5 mM phosphocreatine, 10 mM HEPES, 0.2 mM fluo-3 (Molecular Probes, Eugene, OR), and had calcium added for a nominal $[Ca^{2+}]$ of 100 nM and magnesium chloride added for a nominal $[Mg^{2+}]$ of 0.61 mM. Solutions were titrated to pH 7 and adjusted to 270 mOsmol/kg. Experiments were at 17°C.

Details of chamber design and voltage clamp were given by Shirokova and Ríos (1997) and Ríos et al. (1999). The scanning microscope (MRC 1000, Bio-Rad, Hercules, CA) was in standard fluo-3 configuration (Ríos et al., 1999) and used a 40×, 1.2 numerical aperture water immersion objective (Zeiss, Oberköchen, Germany). Images shown are of fluorescence of fluo-3, determined at 2-ms intervals at 768 points of abscissa x_j along a line parallel to the fiber axis. Fluorescence intensity, $F(x,t)$, was always normalized to the baseline intensity $F_0(x)$, derived as an average of $F(x,t)$ before the depolarization pulse was applied.

Sparks were located automatically (Cheng et al., 1999) by a relative amplitude criterion, separation from the local fluorescence level by more than 2.5 σ_n (standard deviations of the normalized light intensity in the image; González et al., 2000a). We reduced the frequency of false detections by a number of safeguards described by González et al. (2000a). Because the frequency of spontaneous events was extremely low, the frequency of false detections could be estimated (at ~10%) by applying the method to resting images.

Morphological parameters were determined on the detected events as described by González et al. (2000a). In particular, amplitude a was determined as difference between the peak value of the normalized fluorescence and its baseline value at the same spatial position immediately before the event (the average of 10 values between 40 and 20 ms before the peak); full width at half magnitude (FWHM) was determined on the spatial distribution of fluorescence at the time of maximum change, and rise time was determined on a spline interpolate of the time dependent fluorescence, averaged over three spatial pixels at the center of the spark, as the interval between time to 10% increase from pre-event baseline and time to peak.

Single variable histograms are represented by bars or curves (chosen for best visibility) normalized as probability densities. Joint histograms are represented after interpolation by the method of parametric cubic convolution (Park and Schowengerdt, 1983).

THEORY

The relationship between detected and full amplitudes

The goal of this section is to derive the distribution of full spark amplitudes of probability density (pdf) $g(a)$ from the distribution of spark amplitudes (of pdf $f(a)$) in a line scan image. To simplify notation, $f(a)$ represents interchangeably the distribution and its sampling approximation, (normalized) frequency in amplitude histograms. To derive g from f, an expression is first developed for the inverse transformation, which produces f starting from g. To this end we expand work of Shirokova and Ríos (1997), Cheng et al. (1999), and Izu et al. (1998). (Izu et al. (1998) considered the transition from spark strength (intensity or open time of the underlying channels), to observed amplitude. In the present work the spark is taken as a fluorescent object of a given magnitude and time course, and the process of release and diffusion leading to spark formation is not considered).

The theory is valid for analysis of images obtained by line scanning in a direction parallel to the fiber axis. The spread in measured spark amplitudes may result from variation in actual spark size or from variable separation of the spark source relative to the scanned line. In frog muscle sparks originate at triad junctions in the Z disks, of which there is one per sarcomere. A Cartesian coordinate system is defined in which the x axis is the scanned line $(x,0,0)$, x and y are in the focal plane and z is the vertical. In this frame of reference, the Z disk corresponds to the plane $(0,y,z)$. Even though sparks occur there only at triads, one has no information about location of triads relative to the scanning line, which effectively results in homogeneous probability of spatial spark location within y,z space. This property was used, together with the experimentally recorded spark waveform, to generate the amplitude histogram $f(a)$.

Fig. 1 shows in conventional spatio-temporal representation an experimental spark, acquired by line scanning of a voltage-clamped cell, as a fluorescence intensity $F(x,t)$, normalized to the baseline fluorescence $F_0(x)$ and smoothed. (Line scan images from this cell are illustrated in Fig. 4). Because this was one of the largest sparks recorded in the image (and in the experiment) it is reasonable to assume that it originated close to the scanned line $(x,0,0)$, an assumption validated in Appendix B. The spark's amplitude, that is, the peak value of the increase in fluorescence, will be termed henceforth full amplitude, to emphasize that the spark would have been detected with a lower amplitude, had it originated farther from the scanning line. The descriptive term "full" is preferred to "true" amplitude, because

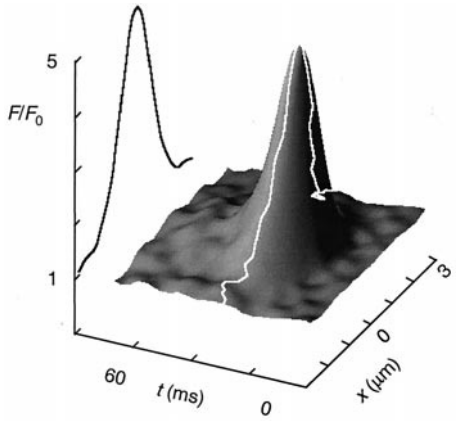

FIGURE 1 Three-dimensional representation of a spark in a line scan. The spark represented was selected from line scan images obtained in a voltage clamp experiment, in which a fiber from the frog semitendinosus muscle, held under voltage clamp at −90 mV, was pulsed to −65 mV for 400 ms. Line scan images are arrays of 768 by 512 fluorescence data points or pixels (F_{ij}), where the index i designates positions along a line and j designates successive scans of the same line, at 0.136 μm, and 2-ms intervals. Represented is a sub-array of 44 × 34 pixels, containing a spark, with fluorescence plotted normalized to resting fluorescence, after two smoothing iterations. The curve in white trace, joins the maxima of the functions of time $F(x,t)$ at constant x. The black trace, obtained by projection of the white trace is $F_{max}(x)$.

even when a spark is ideally centered on the scanning line, its image, $F(x,t)$, is blurred (scaled down and widened).

On the same graph in Fig. 1 the maxima of the functions of time $F(x,t)$ at constant x are joined with a white trace. The black trace, obtained by projection of the curve in white, defines $F_{max}(x)$, which decreases monotonously with x.

Under the assumption that sparks, considered as fluorescent objects, are spherically symmetrical (an assumption valid for most sparks, as shown by video-rate scanning in two dimensions, Brum et al., 2000), $F_{max}(x)$ can be given a different interpretation: it is the amplitude a with which a spark similar to the one shown would be reported, if it originated on the y axis, at distance x away from the scanned line. In other words, $F_{max}(y)$ is the amplitude at which the spark shown would be detected if it originated at $(x,y,0)$ instead of $(x,0,0)$. We therefore use the measured intensity maxima at the x axis ($F_{max}(x)$, detected amplitude function) as a predictor of the downsizing effect of separating scan from spark.

To generalize this approach to three spatial dimensions, a similar use could be made of $F_{max}(x)$ to scale the amplitude when the separation is in the z axis direction. However, the spread of confocal imaging is greater in the axial direction than in the focal plane. This difference was taken into account using the measured point spread function (PSF) of our confocal system (Ríos et al., 1999) as follows:

$F(x,t)$ was first corrected for the blurring produced by the microscope by deconvolving it, at every t value, with the system's x axis PSF (a Gaussian function of x, of FWHM = 0.4 μm). Provided that sparks, as objects, are symmetric, the function thus obtained, $F^*(x,t)$, also describes the dependence of the spark on y and z, as $F^*(\rho,t)$, where $\rho = \sqrt{(y^2 + z^2)}$. $F(y,z,t)$, the blurred image of the spark, was then constructed by convolving $F^*(\rho(y,z),t)$ with the system's two-dimensional PSF (a Gaussian of $FWHM_y = 0.4$ μm and $FWHM_z = 1$ μm). The detected amplitude function $a(y,z)$ (represented in Fig. 2 *A*), was obtained as $F_{max}(y,z)$, the maximum of $F(y,z,t)$ over t at fixed positions y, z. Unlike F^*, $a(y,z)$ is not spherically symmetric. $a(y,z)$ can be imagined as the result of making a radially symmetrical volume from the curve $F_{max}(x)$ and broadening it in the z direction.

$a(y,z)$ is all that is needed to generate the amplitude histogram that would apply if all sparks were equal in morphology to the one shown. Indeed, the function $a(y,z)$ represents recorded amplitude as a function of location, and the probability of occurrence of such locations is simply proportional to the area occupied by such locations in the Z disk (the y,z plane).

Let n be the average number of sparks (all assumed to be equal) produced per unit area of one Z disk. The frequency of measured sparks of amplitude greater than a will be n multiplied by the area of a (roughly elliptical) region, or resel, where the intensity is greater than a (see Fig. 2 *A*). The frequency in an interval da (approximated by the bin value in the amplitude histogram of detected events) is proportional to the area in the ring bounded by two resels, where

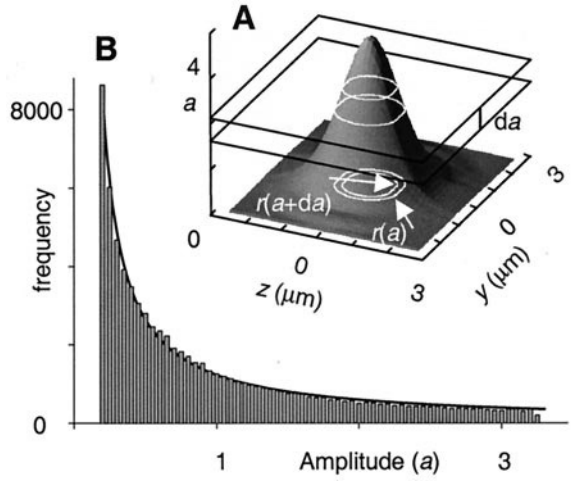

FIGURE 2 Detected amplitudes and their histogram. (*A*) The detected amplitude function, $a(y,z)$, constructed from the function $F_{max}(x)$ (black trace in Fig. 1), essentially by a rotation around the scanning line (x axis, see text). The curves $r(a)$ and $r(a + da)$ mark the regions in the y,z plane where the detected spark amplitude is 0.5 and 0.65 of a_{max}. The frequency of sparks detected with amplitudes in such range is proportional to the area between both curves. (*B*) Histogram of amplitudes detected in a line scan when sparks identical to the one in *A* occur at random locations in the plane y,z. The histogram was calculated with Eq. 1 and n = 25,600 per 4 μm^2. Continuous line is best fit with $f = k/a$.

the amplitude increases by da. Symbolically,

$$f(a)\mathrm{d}a = n\int_{\mathrm{r}(a)}^{\mathrm{r}(a+\mathrm{d}a)} \mathrm{d}y\,\mathrm{d}z \qquad (1)$$

with $r(a)$ and $r(a + \mathrm{d}a)$ representing the two closed curves where the detected amplitude is a and $a + \mathrm{d}a$, respectively.

Eq. 1 can be used as a numerical recipe to calculate the amplitude histogram whenever $a(y,z)$ is known. Using it with the function a represented in Fig. 2 (and $n = 25,600$) the histogram in Fig. 2 was obtained. As described before (Izu et al., 1998; Cheng et al., 1999), the histogram is monotonously decreasing, even though the full amplitude of the sparks is always the same.

The continuous line in Fig. 2 B is the best fit by the function k/a. This one-parameter fit is extremely good over the entire range of amplitudes. A similarly good fit was found for the amplitude histograms generated with all other sparks tested, large or small. The conclusion that the amplitude histogram of a stereotypical spark should follow the reciprocal function was derived analytically by Cheng et al. (1999) and reached through a very different set of considerations by Izu et al. (1998). In Appendix A, we demonstrate that when the detected amplitude function a is a Gaussian function of y and z, with standard deviation σ, the resulting amplitude histogram is exactly

$$f(a) = n2\pi\frac{\sigma^2}{a} \qquad (2)$$

Because the detected amplitude cannot exceed the full spark amplitude $a_{\max}$, Eq. 2 is valid only for $a < a_{\max}$. That the result applies so well to detected functions derived from experimental sparks implies that such functions are close to a Gaussian dependence on y and z.

It is a simple task to generalize this result and determine the amplitude histogram when the object sparks have multiple amplitudes. Assume, first, that there are a few discrete components in the distribution. Specifically, if the frequency of sparks of full amplitude α, $g(\alpha)$, is nonzero only for a finite set of discrete α_j, then the histogram of amplitudes in the line-scan, $f(a)$ can be written as a sum of discrete contributions of form (2) for each of the subgroups of amplitude α_j

$$f(a) = 2\pi\sum_{j,\alpha_j\geq a} g(\alpha_j)\frac{\sigma_j^2}{a} \qquad (3)$$

This formulation is useful for the theoretical analysis, but not essential in practice, as the function $f(a)$ can also be constructed by addition of discrete terms of form (Eq. 1).

When the distribution of full amplitudes is continuous, Eq. 3 becomes:

$$f(a) = 2\pi\int_a^\infty g(\alpha)\frac{\sigma(\alpha)^2}{a}\,d\alpha \qquad (4)$$

Eq. 4 can be interpreted as an integral transform, in which the experimental histogram $f(a)$ is expressed as an integral of generator functions $(\sigma(\alpha)^2/a)$, with coefficients $g(\alpha)$. In this sense, the goal of this section is to invert such transform. This is accomplished solving Eq. 4 for $g(\alpha)$ by differentiating the integral with respect to the first limit of integration:

$$\frac{\mathrm{d}(af(a))}{\mathrm{d}a} = 2\pi\frac{\mathrm{d}}{\mathrm{d}a}\int_a^\infty \sigma^2(\alpha)g(\alpha)\mathrm{d}\alpha = -2\pi\sigma^2(a)g(a) \qquad (5)$$

or, in a practical form,

$$\sigma^2(a)g(a) \propto \frac{\mathrm{d}(af(a))}{\mathrm{d}a} \qquad (6)$$

Note that it is essential for the derivation to distinguish between detected amplitude a and full amplitude α. The disappearance of the argument α in the final expression of Eq. 6 reflects the fact that the full amplitude is not known for individual sparks, and the algorithm yields only its distribution, g.

A test of the algorithm with simulated distributions

Eq. 6 is the relationship sought between g, the distribution of full amplitudes, and the amplitude histogram f of events in a line scan. It is strictly valid only when the detected amplitude function $(a(y,z))$ is Gaussian. This is not true in general, but appears to be a good approximation in most cases. Moreover, the half-width of sparks is poorly correlated with amplitude, both for experimental sparks (as shown by González et al., 2000a; see also Discussion) and in simulations (Ríos et al., 1999), suggesting that the Gaussian σ in Eq. 6 may be regarded as constant in a first approximation. The algorithm in Eq. 6 should therefore work as an approximate way of deriving g in real situations. In the remainder of this paper, the right-hand side of Eq. 6 is presented normalized as a probability density, and referred to as g or corrected amplitude distribution. (Normalization is done dividing the right-hand side of Eq. 6 by the integral of its non-negative portion over the whole amplitude range and by the binning interval. Negative values of g arise wherever $a\,f(a)$ increases with a, presumably due to noise or imperfect detection.)

The procedure was tested by applying it to amplitude histograms derived from known (simulated) distributions of sizes, using actual, experimentally recorded sparks.

Fig. 3 illustrates the test. At the top in Fig. 3 A is a histogram of detected amplitudes (thick trace), calculated numerically assuming that there are only three subpopulations of sparks: one of them is composed of clones of that in Fig. 1, of full amplitude 3.25. The other two sets are clones of two other sparks from the same experiment, with full

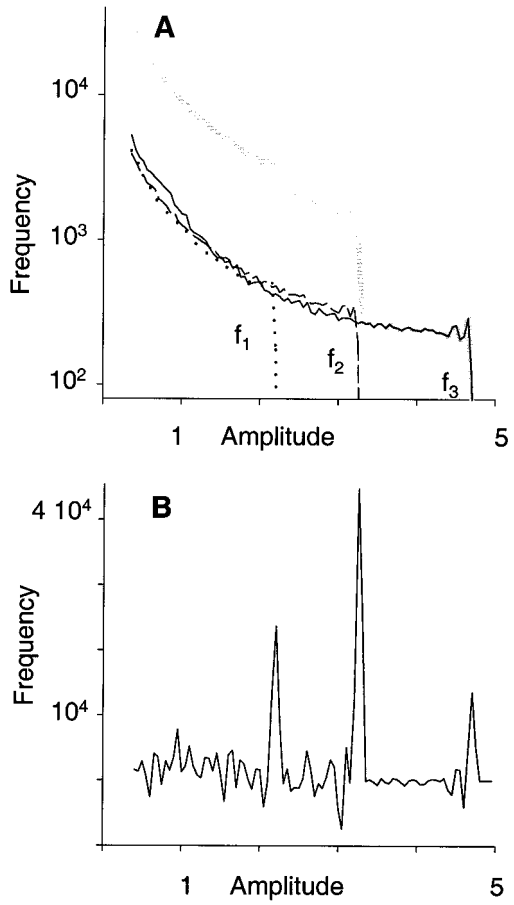

FIGURE 3 A test of the algorithm for derivation of amplitude distribution. (*A*) Amplitude histograms from the spark in Fig. 1 (f_2) and two others from the same experiment (f_1 and f_3). The contributions, calculated with Eq. 1, are similar up to a limiting detected amplitude, which in each case is equal to the full amplitude of each original spark (the α_j values of Eq. 3, approximately 2.2, 3.25, and 4.7). The thick curve is the joint histogram ($2f_1 + 4f_2 + f_3$), calculated according to Eq. 3 with frequencies $g(\alpha_1) = 2$, $g(\alpha_2) = 4$, and $g(\alpha_3) = 1$. (*B*) Distribution of full amplitudes, $\sigma^2 g(a)$, calculated from the joint histogram according to Eq. 6. Note agreement between $g(\alpha_j)$ used to generate the histogram at top and that recovered by the algorithm (where the peaks are in the approximate relationship: 2, 4, 1).

amplitude 2.2 in one case and 4.7 in the other. Curves f_1 to f_3 in Fig. 3 *A* represent the individual contributions of each set to the amplitude histogram, calculated assuming equal n for each set. The contributions are similar up to a limiting detected amplitude, which in each case is equal to the full amplitude of each spark (the α_j values of Eq. 3, namely 2.2, 3.25, and 4.7). If the detected amplitude functions of these sparks were Gaussians of equal σ, these contributions would be functions k/a, exactly overlapping up to the corresponding α_j. They do not exactly overlap because they were derived from real sparks.

The curve in thick trace was obtained according to Eq. 3, by linear combination of the f_j values with coefficients $g(\alpha_1) = 2$, $g(\alpha_2) = 4$, and $g(\alpha_3) = 1$, chosen arbitrarily to have a mode in the discrete distribution $g(\alpha)$, at the intermediate amplitude 3.25. This is, therefore, an amplitude histogram derived from actual experimental sparks and a simulated distribution.

To this histogram we applied Eq. 6. If the detected amplitude functions were Gaussian, the result would be exactly $\sigma^2 g(a)$. The result is plotted in Fig. 3 *B*. The procedure recovered three peaks, at the correct amplitudes, with ordinates of relative values 1.74, 3.29, and 1 (close to the starting g values of 2, 4, and 1). An even better agreement is found by integration of the areas under the three peaks, which yields relative values of 1.95, 3.50, and 1. Discrepancies are expected, because the individual histograms are not exact reciprocal functions (k/a), and because the algorithm recovers the distribution function $g(a)$ multiplied by the width parameter σ^2, which is not strictly a constant. A test with a smaller number of sparks ($n = 1024$) gave three peaks of similar relative values, on a noisier baseline, especially at low values of a.

RESULTS

In the previous section a method was developed to derive the true distribution of amplitudes, starting from their distribution in confocal line scans. The method was then tested, with good results, on histograms derived from experimental sparks, but with an assumed (arbitrary) distribution.

In this section we use the algorithm on actual histograms of experimental sparks. The true distribution in these cases is unknown, and therefore the adequacy of the algorithm cannot be assessed with certainty. To test the algorithm we took advantage of the fact that two other morphometric parameters of the spark, rise time and width, can be determined with more certainty than the amplitude. Modeling by several laboratories has shown these two parameters, especially rise time, to be less affected by off-focus errors (Pratusevich and Balke, 1996; Smith et al., 1998; Jiang et al., 1999).

For many sets of sparks, especially but not necessarily in the presence of caffeine, the distribution of rise times exhibited a clear mode (González et al., 2000). In these cases the true distribution of amplitudes should also have a mode. Indeed, rise times of sparks are essentially the times when the underlying release process is active. Hence, if release times (open times of the release channels) are stereotyped or modal, true amplitudes are expected to have a preferred value as well (or a dearth of the very small events resulting from very short open times, which effectively results in at least one mode in the amplitude distribution). This expectation does not rely on any assumption about the number of channels involved in one spark.

This section compares first the presence of modes in the corrected amplitude distributions and in the distribution of rise times. Later, comparisons are extended to joint distributions of rise time and width.

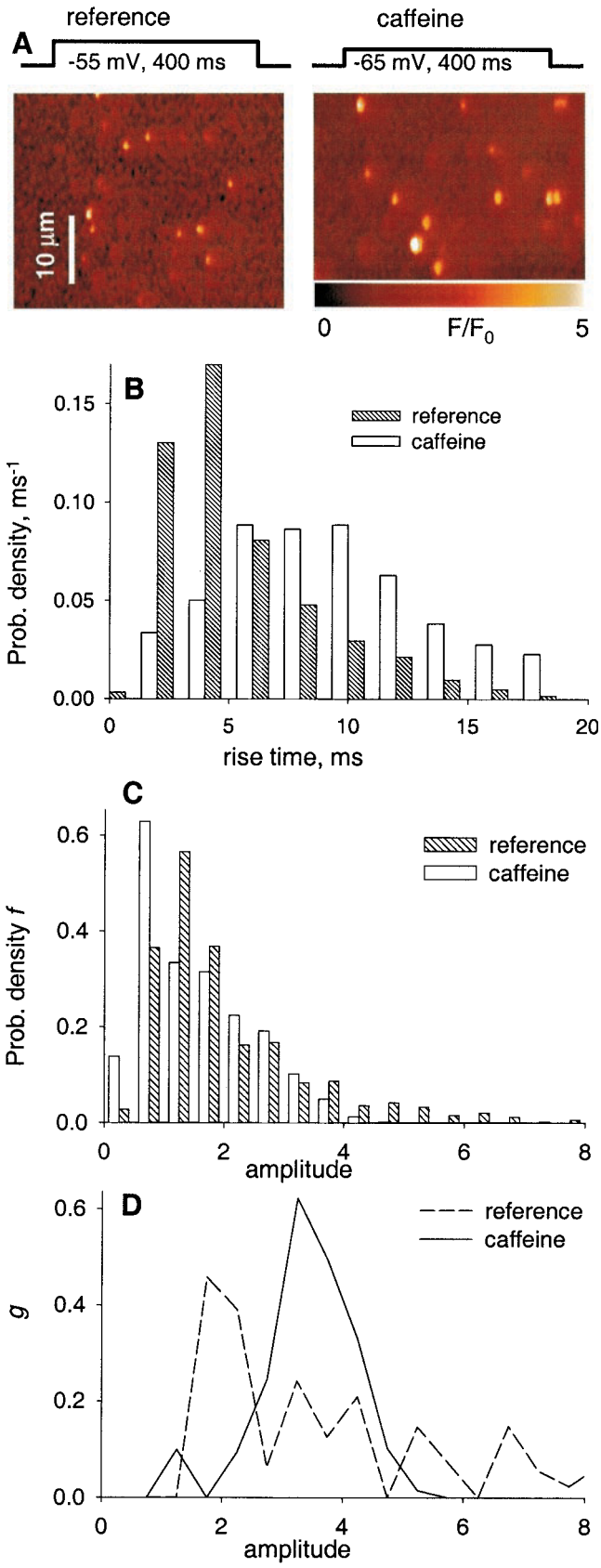

Amplitude distributions in the presence of caffeine

Two studies (González et al., 2000a,b) demonstrated that fibers in caffeine often exhibit a mode in the distribution of rise times. The same experimental database is analyzed here for distributions of amplitudes and widths. As described in detail by González et al. (2000a), spark properties were studied in multiple line scan images, obtained at different locations in a voltage-clamped fiber. Fig. 4 *A* illustrates images obtained from the same cell, in reference solution, and after addition of 1 mM caffeine. The fibers, prepared as described in Methods, had no or few spontaneous sparks. Depolarizing pulses of long durations were applied at 1-min intervals, to voltages near −60 mV in reference, sufficiently high to maximize the numbers of events while keeping them sufficiently separate to avoid overlap and increase in global fluorescence. The pulses applied in the presence of caffeine were typically of 5 or 10 mV lower amplitude to avoid increasing event frequency. Sparks were located automatically, using a relative amplitude criterion (see Methods).

In the experiment illustrated, 548 events were detected in 7 images in reference, and 883 events in 10 images obtained subsequently, in the presence of 1 mM caffeine. (Large numbers of events, detailed in the table, are the rule for all distributions shown.) Fig. 4 *B* shows a broad mode in the histogram of rise times in the presence of caffeine. Evidence that this mode is real, rather than an artifact of limited detection of smaller events, was given by González et al. (2000b). In Fig. 4 *C* are the corresponding histograms of amplitudes. As predicted by the theory, the distribution of amplitudes is decreasing. The mode in the third bin is a trivial artifact of failed detection of the smallest events, as it moves to the left when the detection criterion is lowered (González et al., 2000b; Cheng et al., 1999). The measurable frequency of events of amplitude >5 in reference, but not in caffeine, was an unusual observation.

Fig. 4 *D* represents the functions $\sigma^2\, g(\alpha)$, obtained from the amplitude histograms by the correction algorithm, Eq. 6, and normalized as a probability density; we refer to these functions simply as "corrected distributions" or $g(a)$. A clear mode, at an amplitude ~4, was present in caffeine but not in reference; the small peak at low amplitudes should be

FIGURE 4 The distribution of rise times and amplitudes. (*A*) Representative line scan images of fluorescence, normalized to its time-averaged value at holding potential, taken from the same voltage-clamped cell in reference solutions (*left*), or in the presence of 1 mM caffeine. Note the stimulus voltage: −55 mV in reference and −65 in caffeine. (*B*) Rise time histogram of 548 events in reference (*hatched bars*) or 883 events in caffeine (*open bars*). Events were detected automatically in 7 images in reference and 10 images in caffeine. Rise time was measured on every detected event as described in Methods. (*C*) Amplitude histograms ($f(a)$) of the same events. (*D*) Corrected amplitude distribution, $g(a)$, calculated from the $f(a)$ using Eq. 6. Note appearance of a mode in caffeine (*solid line*). Fiber identifier 0315a (studied by González et al., 2000b).

disregarded, as it reflects detection limits. The mode was robust upon several procedural changes, including changes in binning interval or starting value, and in the amplitude threshold for detection (illustrated later). The mode was also present when an absolute amplitude criterion, rather than one relative to noise, was used for detection (Cheng et al., 1999). As documented in Table 1, the appearance of a mode in caffeine was quite reproducible, and the mode location is representative of that found in several experiments.

The presence of a mode in the corrected distribution of amplitudes did not require caffeine. However, it did correlate very strictly with the presence of a mode in the distribution of spark rise times. Figs. 5 and 6 illustrate two examples. At top in Fig. 5 is the histogram of rise times for 923 events in 12 images in reference (no caffeine was applied in this experiment), featuring a mode at 6 ms. The histogram of amplitudes, Fig. 5 *B*, is monotonically decaying, whereas the corrected distribution, Fig. 5 *C*, features a clear mode at amplitude 6.

Modes in the distribution of amplitudes are statistically significant

The example in Fig. 5 illustrates two tests of the significance of the mode in the corrected distribution. $g(\alpha)$ results from the differentiation of $a\,f(a)$ (Eq. 6), so that a mode in g corresponds to a large jump in $a\,f(a)$. To test the statistical significance of the change in $a\,f(a)$ we compared the running difference $\Delta af \equiv (a_i f(a_i) - a_{i-1} f(a_{i-1}))$ with ϵSD, an estimator of its standard error, calculated assuming that the bin frequencies in $f(a)$ have a Poisson distribution (e.g., Reif, 1962), as $\epsilon\text{SD} = \sqrt{(a_i^2 f(a_i) + a_{i-1}^2 f(a_{i-1}))}$. In the null hypothesis that Δaf is zero (implying that all sparks have one and the same amplitude), the ratio $\Delta af/\epsilon$SD should have approximately a t distribution. Its number of degrees of freedom, $n(f(a)_I + f(a)_{I-1})$, is >20 at the amplitudes of interest, so that the t distribution is indistinguishable from a Gaussian.

$\Delta af/\epsilon$SD is plotted versus amplitude in Fig. 5 *D*. It appears not to have a t distribution, as it is positive at all but one value of a. This suggests that the null hypothesis may be wrong at all amplitudes; in other words, g is probably different from zero in the range of amplitudes represented—there are sparks of many different amplitudes. It is only at $a = 6$, however, that $\Delta af/\epsilon$SD is different from 0 at a $P < 0.05$ (in fact, $P < 0.0005$), indicating that the mode in g is probably real, not due to the limited size of the sample.

An additional test relied on the fact that a mode not determined by noise should remain upon increasing noise. The set of events was divided randomly into two sets of half the size, and the correction algorithm was applied to the amplitude histograms of the half-sets, yielding the two dashed plots in Fig. 5 *C*. Other divisions in two of the original set gave similar results. This procedure is roughly equivalent to increasing noise in the histograms by a factor of $\sqrt{2}$. Whenever Δaf was greater than 3 ϵSD, the mode

TABLE 1 Modes in the distribution of spark amplitudes and rise times

1	2	3	4	5	6	7	8	9	10	11
	Number of events		Amplitude (g) mode location		Mode significance		Rise time (ms) mode location		Amplitude average	
Fiber	ref	caff	ref	caff	ref	caff	ref	caff	ref	caff
0605a	1029		none				2.7			
0608b	923		6.0			yes	6.0		3.17	
0414a	735	176	3.0	3.5	no	yes	2.7	3.3	1.21	1.27
0414b	1105	506	none	3.2		yes	2.7	3.3		1.28
0507b	581	273	3.8	3.8	yes	yes	4.0	8.7	1.87	1.97
0522a	407	211	none	3.0		no	2.7	2.7		1.54
0605b	266	427	none	none			2.7	2.7		
0608c	410	427	4.0	5.3	yes	yes	4.0	6.0	1.46	1.45
0315a	548	883	none	3.5		yes	4.0	8.0		1.55
0315b	923	1211	none	4.5		yes	2.7	2.7		2.11
0329a	385	802	5.0	4.5	no	yes	2.7	6.0	2.02	2.48
Mean			4.36	3.91					1.95	1.71
S.E.M.			0.52	0.28					0.34	0.15

Headings "ref" and "caff" designate data in reference and in the presence of caffeine. In columns 4 and 5 are the locations of modes in the distribution g of spark amplitudes. Columns 6 and 7 list the significance of these modes, established as described in the text. Columns 8 and 9 list the locations of modes in rise time histograms of the same sets of events (the nominal resolution of rise times, and binning used, was 0.667 ms, cf. González et al., 2000a). Columns 10 and 11 give average measured amplitude, for the sets that had a mode in g. Fibers in the group at top (2) were not exposed to caffeine. Those in the middle group (6) were exposed to 0.5 mM and in the bottom group (3) to 1 mM caffeine. For the experiments in 0.5 mM caffeine, the reference events include those obtained in washout runs.

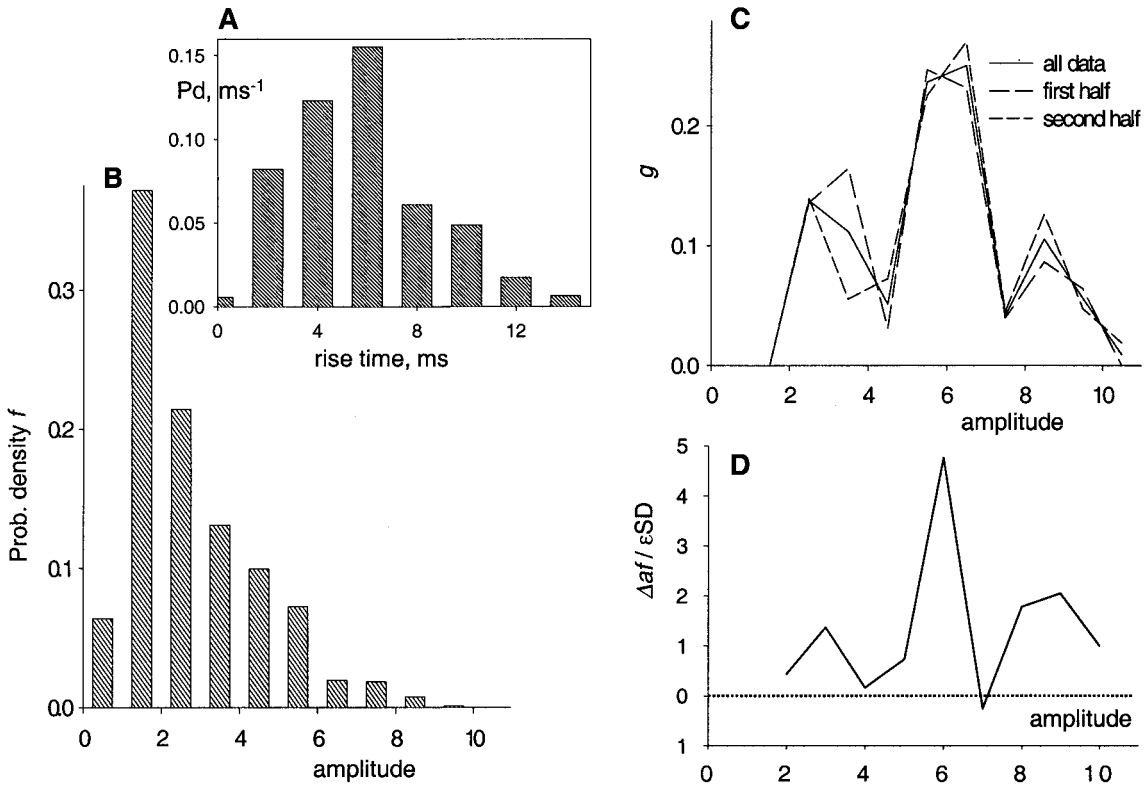

FIGURE 5 Modal distribution of amplitudes. (*A*) Rise time histogram of 923 events detected in 12 images in reference condition, elicited by pulses to −65 or −70 mV. (*B*) Amplitude histogram of the same events. (*C*) Corrected amplitude distribution *g*, derived from the amplitude histogram (*solid line*). The *g* distributions represented with dashed lines were derived from histograms of amplitudes of two mutually exclusive subsets, of 461 and 462 events, randomly selected from the full set. (*D*) Amplitude dependence of the statistic $\Delta af/\epsilon SD$ (the difference between successive bin values of $a\,f(a)$, divided by its standard error, defined in the text), which should have a Student's *t* distribution with *n* degrees of freedom wherever $g(a) = 0$. *n*, the number of events in the two neighboring bins of the amplitude histogram, is 30 or greater at all $a < 8$. Identifier: 0608b.

was robust upon halving the sample size. Both tests are, therefore, approximately equivalent indications that the modes correspond to actual features in the distribution of amplitudes.

Correlation between modes in amplitude and rise time

Although $g(a)$ was usually modal in the presence of caffeine, the situation in reference conditions was quite variable. A monotonic distribution was illustrated in Fig. 4 and a modal one in Fig. 5. Fig. 6 illustrates an experiment in which the events recorded before caffeine had a modal distribution *g*; the mode became more marked in the presence of caffeine, and disappeared upon washout. In remarkable agreement, the distribution of rise times (Fig. 6, *A–C*) had a well defined mode in the presence of caffeine, one less marked in the reference situation before caffeine, and appeared to be monotonic upon washout.

Results in multiple cells are listed in Table 1, where the headings "ref" and "caff" identify the condition. Columns 2 and 3 list the numbers of events detected in each case. Columns 4 and 5 list the location of the mode, if present, in the corrected distribution of amplitudes. Columns 6 and 7 note the significance of these modes, determined by the two tests described above. Columns 8 and 9 give the locations of the modes in the distributions of rise times for the same sets of events.

The table indicates that 5 of 11 cells in reference had a mode in $g(a)$. Nine of these cells were exposed to caffeine. In four of those the mode was not present in reference but all but one developed a mode in caffeine. In two of the others the mode, which was present but not significant in reference, became significant in caffeine. Even when the mode was significant in reference, it increased in density and definition in caffeine. The abscissa of the mode decreased slightly in caffeine.

The table also lists the location of the modes in rise time distributions. As shown in Figs. 4–6, a mode is always present in those distributions. However, it is usually at one of the first few bins in the histograms, where it may be due to failure of detection of very brief events. González et al. (2000b) concluded that modes located at times greater than 4 ms are probably real, and the present comparison indi-

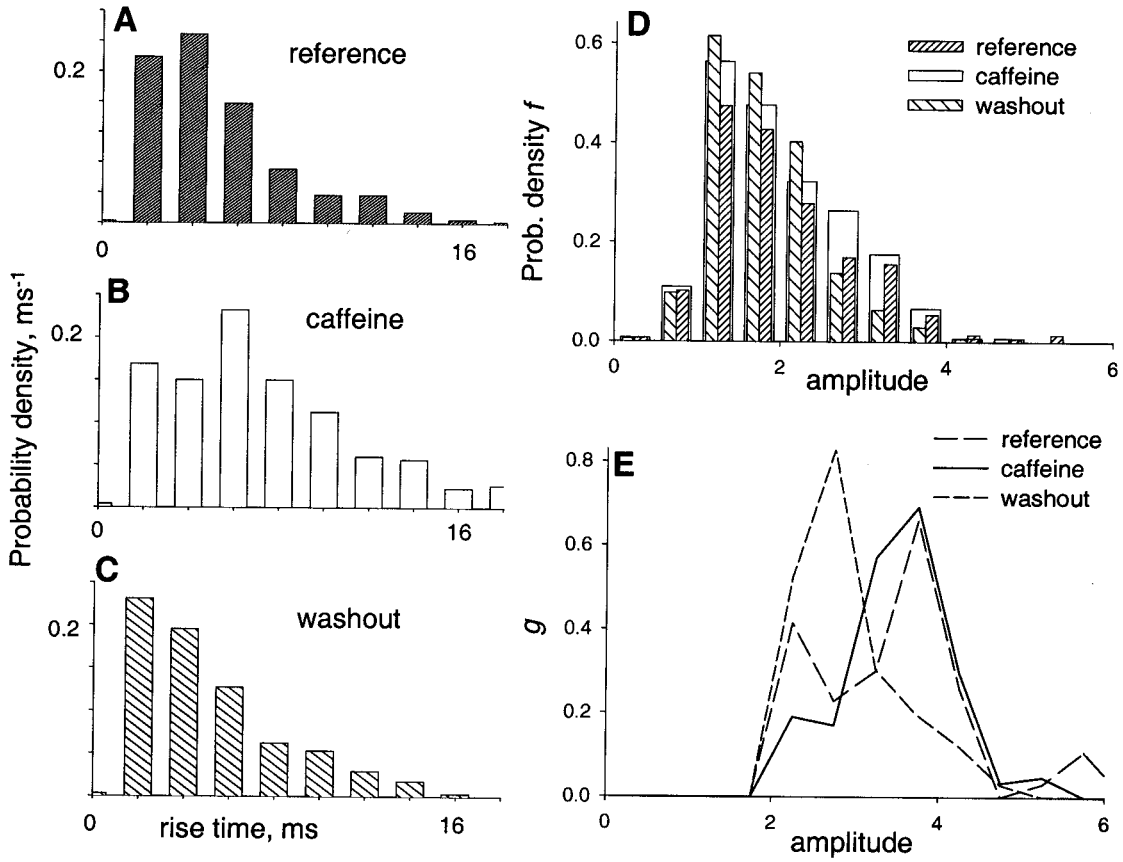

FIGURE 6 Effects of caffeine. (*A–C*) Rise time histograms of events detected in reference condition (*A*, 250 events, 5 images), during a subsequent exposure to 0.5 mM caffeine (*B*, 273 events, 4 images) and after washout (*C*, 331 events, 6 images). (*D*) Amplitude histograms of the corresponding sets. (*E*) Corrected amplitude distributions (*g*). Note correspondence between presence of mode in the rise time and *g* distributions and disappearance of modes after washout. Identifier: 0507b.

rectly agrees with that conclusion. When the modes of rise times were at less than 3 ms, there was either no mode in *g* or the mode was not significant. When the mode was at greater than 4 ms, the mode in *g* existed and was significant. The simplest interpretation is that the presence of modes in the distribution of rise times results in modal distributions of amplitude, and that the modes at rise times greater than 4 ms and those present in the $g(a)$ graphs correspond to real features (preferred open times and amplitudes) of the sets of events. Borderline cases, when rise times were grouped around 3 or 4 ms, are clarified by the analysis of joint distributions.

The joint distribution of rise time and width

As stated, the measured amplitude of sparks depends strongly on the position of the source relative to the scanning line. Therefore the strategy of the previous sections was to compare the corrected amplitude distribution with the much more robust distribution of rise times. Because spark spatial width increases with source intensity and open time (as does spark amplitude), the measurement of width (FWHM) provides an independent test of the adequacy of the amplitude correction algorithm.

Joint histograms of rise time and width, especially after interpolation by the cubic convolution procedure of Park and Schowengerdt (1983), reveal more clearly the presence of modes than the single variable histograms (González et al., 2000a). For this reason, the features of the joint distribution exhibit a much more detailed correspondence with modes in $g(a)$ and help clarify cases when the modes in rise times are dubious.

A first example is illustrated in Fig. 7, an experiment in which both the distribution of rise times and the $g(a)$ had a mode in reference. However, the mode of rise times at the second bin of the histogram (2–4 ms) was suspect. The joint histogram in reference, Fig. 7 *A*, shows two modes, termed "large" and "small" for brevity: "small" at a rise time of 2.5 ms and a width of ~0.9 μm, and "large" at ~4.5 ms and 1.8 μm. In good correspondence, the amplitude distributions $g(a)$, plotted in Fig. 7 *D*, feature two modes in reference. In 0.5 mM caffeine, Fig. 7 *B*, the joint histogram features only

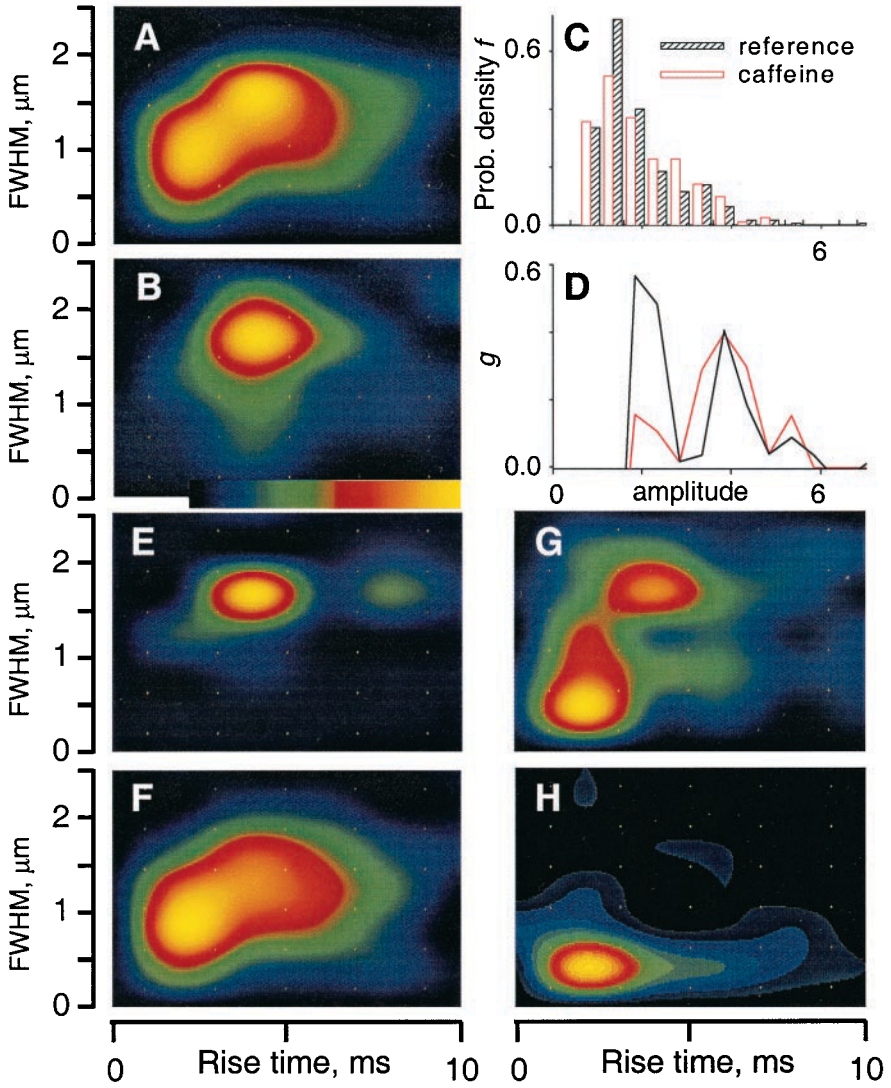

FIGURE 7 The joint distribution of rise time and width. (*A*) Joint histogram of rise time and full width at half magnitude, for all 412 events detected in a cell in reference. (*B*) Joint histogram for all 427 events in the same cell exposed to 0.5 mM caffeine. Note bimodal distribution in reference, and disappearance of the small mode in caffeine. (*C*) Amplitude histograms in both conditions. (*D*) Corrected amplitude distributions $g(a)$. Note presence of two modes in reference, and near disappearance of the low amplitude mode in caffeine. (*E*) Joint histogram of events in reference whose measured amplitude was >3. Note exclusive mapping to the large mode. (*F*) Events whose amplitude was ≤ 3. (*G*) Histogram of events in caffeine, with a threshold criterion lowered to 2 σ_n. Note appearance of a mode at low rise time and width. (*H*) Events detected in images at the holding potential, obtained in the presence of caffeine. A similar result, not shown, was obtained in reference. Binning intervals for joint histograms are 0.428 μm and 2 ms. Maxima in color scale are 32, 30, 14, 30, 32, and 15, respectively, for *A*, *B*, *E*, *F*, *G,* and *H*. The histograms are plotted after interpolation by the cubic convolution method of Park and Schowengerdt (1983). Identifier: 0608c.

the large mode, as if most events in the small mode had become large. This corresponds well with the change in $g(a)$ (Fig. 7 *D*), which in caffeine exhibits essentially a single mode, with the same abscissa as the one at greatest a in reference. Hence, the joint histograms exhibit a detailed correspondence with the corrected amplitude distributions and clarify that the single mode in the rise time histogram in reference really includes two modes or types of events, the nature of which is explored later.

The correspondence between the number of modes in the joint histograms and that in $g(a)$ would be meaningless if modes in amplitude did not map onto the modes in the joint histogram. Fig. 7, *E* and *F*, illustrates such mapping. Events in reference were separated in two groups, of measured amplitude greater or less than 3 (the value that separates the peaks in $g(a)$, Fig. 7 *D*). In Fig. 7 *E* is the joint histogram of events with amplitude greater than 3. As expected, most of them map to the large mode in the joint histogram.

Due to the nature of the correction, the mapping is not bijective (or one-to-one). In Fig. 7 *F* is the joint histogram of the events of amplitude less than 3. This group does not and should not map specifically to the small mode. Indeed, events can have low measured amplitudes because they are truly small (mapping to the mode of lower rise time and width), or because they are large but off-focus (belonging to the large mode of the joint distribution). The mapping between modes in g and modes in the joint histogram, therefore, indicates that the algorithm works correctly.

Of the two modes in the joint distribution, the small one probably reflects a group of smaller events whose distribution is curtailed by limited detection. When the threshold for detection was lowered to $2\sigma_n$ (cf. Methods), a small mode appeared in caffeine (Fig. 7 *G*). Moreover, when the detector was applied with lowered threshold to images obtained at the holding potential, only the small mode was left (Fig. 7 *H*) indicating the presence of false events in this mode.

The large mode, instead, was robust upon change in detection threshold (Fig. 7 *G*), and essentially devoid of false events (Fig. 7 *H*), both indications that it is not artifactual (González et al., 2000b).

When the joint distribution failed to show modes, so did the corrected distribution of amplitudes. Fig. 8 illustrates two examples. In Fig. 8 *A* is the joint histogram of a cell that was studied in reference only, exhibiting a widely spread distribution, with many events of long rise times but only the trivial small mode. The density $g(a)$, in Fig. 8 *B*, is monotonically decreasing from a peak at low amplitude. This agreement was the rule. The other panels in the figure contain the joint histograms for the experiment in Fig. 4, in which the corrected density $g(a)$ was monotonous in reference, but had a mode in 1 mM caffeine (Fig. 4 *C*). Accordingly, the joint distribution went from having just the small mode in reference, at rise time between 2 and 3 (Fig. 8 *C*), to having an additional broad mode in caffeine (Fig. 8 *D*). In this situation, all events of amplitude >2 (belonging to the caffeine-induced mode in $g(a)$) mapped onto the new mode in the joint histogram (image not shown). As was the case for the experiment in Fig. 7, the events of amplitude <2 did not map to either mode in the joint histogram.

DISCUSSION

This paper communicates an advance in the theory of line scanning of Ca^{2+} sparks, which made possible a new method of analysis and led to a new experimental observation. We extended the theory of imaging by confocal scanners (Pratusevich and Balke, 1996; Shirokova and Ríos, 1997; Izu et al., 1998; Cheng et al., 1999) to derive the mathematical form of the histogram of spark amplitudes. Using a numerical computation (Eq. 1) based on the detected amplitude function (Fig. 2), we showed that the amplitude histogram $f(a)$ is well approximated by an inverse proportionality, k/a, when all sparks are identical. Using this approximation we could then define an algorithm (Eq. 6) to recover the true distribution of spark amplitudes from the amplitude histogram experimentally determined in line scans. When applied to amplitude histograms from sparks with a modal distribution of rise times (which was generally the case in cells exposed to caffeine), the algorithm produced amplitude distributions with a mode.

The algorithm yields the function $\sigma^2 g(a)$, where σ is the standard deviation of the approximating Gaussian. Therefore, the result is not strictly an amplitude distribution. For example, if the true distribution consisted of some small and narrow sparks, and others that were large and wide, then the algorithm would overestimate the frequency of large sparks. The parameter σ that appears in Eq. 6 is the true width, the one reported when sparks are centered on the scanned line. The width of the largest sparks in any given image varies within a narrow range. Consequently, the result of the algorithm is approximately proportional to $g(a)$.

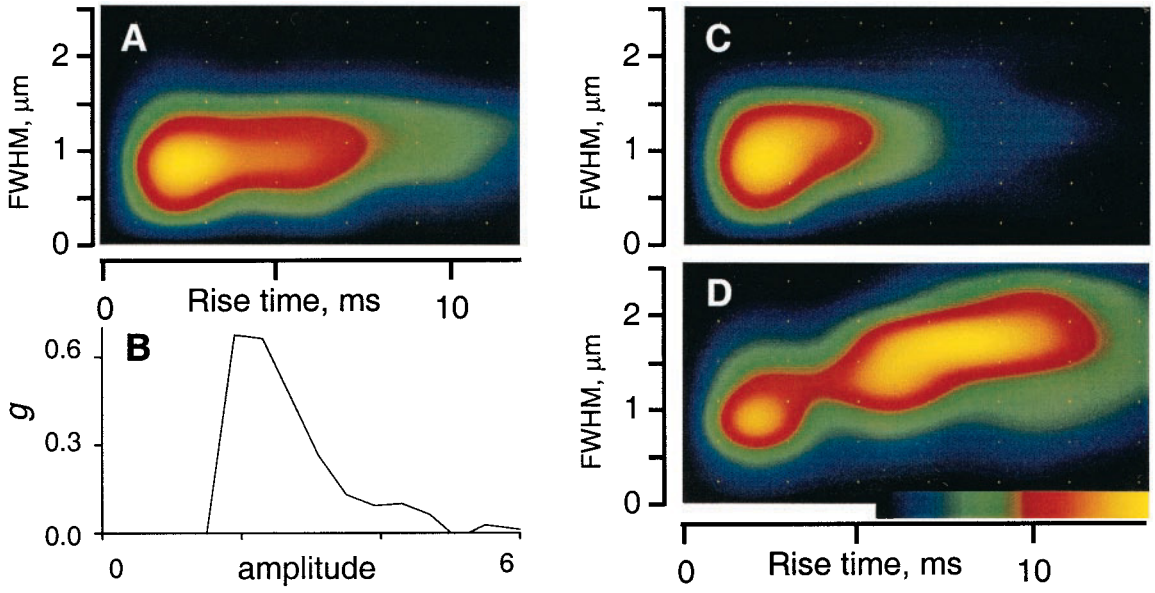

FIGURE 8 Joint distributions with trivial modes. (*A*) Joint histogram of rise time and width for all 1029 events detected in a cell in reference. Note the presence of a single mode, which qualifies as artifactual for being at a low value of rise time. (*B*) The corrected amplitude distribution, decaying after a low amplitude maximum. This fiber was not exposed to caffeine. (*C* and *D*) Joint histogram for events in reference, or in caffeine, in the cell whose amplitude distributions are illustrated in Fig. 4. Similar to that in *A*, the reference histogram *C* has only the trivial mode. This corresponds well with the monotonically decaying $g(a)$ in Fig. 4 *C*. In caffeine (*D*), the histogram becomes bimodal, and the amplitude distribution develops a large mode at amplitude ~4. Binning intervals for joint histograms are 0.428 μm and 2 ms. Maxima in color scale are 176, 90, and 75 events, respectively for *A*, *C*, and *D*. Identifiers: 0605a and 0315a.

Tests of the correction algorithm

The algorithm was tested successfully (Fig. 3) on histograms constructed using experimental sparks, rather than the Gaussian idealization that makes the algorithm exact. The test proved the mathematical consistency of the algorithm, and was an independent verification of goodness of the assumptions (including Gaussian profile of sparks, their approximately constant spatial width, and the random location of their sources within the plane of the Z disks).

When the algorithm was applied to experimental amplitude histograms, the resulting density $g(a)$ was positive at almost every measured value of a (consistent with the presence of events of every amplitude, that is, a continuous distribution of true event amplitude within the measured range) and had a mode in many cases. The mode could be a simple artifact of noise in the histograms. To test this hypothesis the value of $g(a)$ (strictly, of the change in $a\,f(a)$, proportional to $g(a)$) was compared with its probable error. The $g(a)$ value was significantly different from zero only at or near the modal amplitude, which suggests that the mode is not fortuitous. In a related test, the modes were found to be still present when noise in the histogram was increased by halving sample size. These tests effectively ruled out noise as a determinant of the mode.

The algorithm cannot undergo a rigorous test on experimental data because the true amplitude distribution of experimental sparks is unknown. To circumvent this problem, we relied on a fact first indicated by Pratusevich and Balke (1996) and confirmed under different assumptions by others (Smith et al., 1998; Jiang et al., 1999), namely, that rise times and, to a lesser extent, spatial widths are robust under line scanning, varying little with the distance between scanning line and spark origin.

In other words, one may know rise times and widths with reasonable certainty, even for out-of-focus sparks. Hence, if a mode is present in the distribution of rise times, then events of very low amplitude, corresponding to very short rise times, should be comparatively less frequent. This should result in a distribution whose pdf increases with amplitude at low values of the amplitude. Hence, if the correction algorithm was adequate, it should produce a $g(a)$ with a mode. Indeed, there was an excellent correlation between the presence of a mode in the distribution of amplitudes and in that of rise times.

In some cases the result of the comparison was inconclusive, usually because a mode at low values of rise time could be artifactual. In these cases the joint distribution of rise time and spatial width often exhibited two modes, of which one (small) was artifactual and the other was robust upon changes in detection sensitivity and/or binning. Whenever a significant mode was present in the joint distribution, the density $g(a)$ exhibited a clear mode at large a. Moreover, there was the expected mapping: the events that were large and closer to focus, i.e., those with an amplitude near the large mode in $g(a)$, mapped exclusively to the large mode in the joint histogram.

The success of the test with simulated distributions, together with the observed correlation between the presence of modes in rise times, widths and amplitudes, indicate that the algorithm is qualitatively correct. At the same time, the result reinforces the conclusion (González et al., 2000b) that the modes in rise time, observed not only in the presence of caffeine, but also in some experiments in reference, are real, rather than artifacts of the detection procedure. (The correspondence between amplitude and rise time distributions may be used conversely, to argue that events of greater rise time tend to have greater amplitude. This statement, however, would only apply to full amplitude, which is unknowable for an individual event. For measured amplitudes, the off-focus error may be so large that the correlation is lost, as suggested by observations of González et al. (2000b) and Lacampagne et al. (1999).)

Modal rise times require irreversible gating

The significance of a mode in the distribution of rise times has been discussed previously (Cannell and Soeller, 1999; Bridge et al., 1999; González et al., 2000a). Its presence is not explicable if sparks are due to the opening of one Markovian channel evolving reversibly (a channel whose transition rate constants depend on the present state only, and in addition satisfies microscopic reversibility, e.g., Colquhoun and Hawkes, 1995), because the open time distributions of such channels are sums of decaying exponentials. By contrast, a channel that evolves irreversibly can have modal open time distributions (Colquhoun and Hawkes, 1995). Channels that gate irreversibly have been identified (Schneggenburger and Ascher, 1997; Chen and Miller, 1996), but we know of only one example in the literature of a channel with nonmonotonic open time distribution (Gration et al., 1982). In support of the possibility of irreversible gating, the Ca release channel is known to be regulated by the permeating ion (Tripathy and Meissner, 1996; Xu and Meissner, 1998), and therefore has the capability to derive energy from the $[Ca^{2+}]$ gradient and evolve irreversibly. A model that features interaction with the permeating ion has been developed by Wang et al. (2000) and shown to have stereotyped rise times. These simulations, however, must be considered only a theoretical demonstration of possibilities, because the actual distributions of open times in bilayers, for channels conducting Ca^{2+}, do not have clear modes (Wang et al., 2000).

The couplon model produces modal amplitudes

A mode in the amplitude distribution comes naturally instead, assuming that groups of channels underlie sparks, as argued by Shirokova et al. (1999). For example, in the

couplon model (Stern et al., 1997) sparks are produced by arrays of sarcoplasmic reticulum channels (couplons) along one side of a junctional segment (Franzini-Armstrong and Jorgensen, 1994) of transverse tubule. In simulations the sparks from a couplon of 28 channels and 0.3 pA unitary current had multiple amplitudes (due to the stochastic variation in the number of channels involved in individual sparks, as well as the variable open times), but with a clear mode in their distribution, at amplitude 1.3 (Fig. 18 of Stern et al., 1997). When we repeated the simulation with unitary current of 1 pA (which could be closer to the value in frog muscle; Kettlun et al., 2000) the mode moved to an amplitude ~4.0. An additional source of variation in amplitude would be the spread in couplon size, resulting in an overall distribution that, in reference, might not have a mode. Therefore, the couplon model explains qualitatively the presence of a mode in the distribution of amplitudes, and generates sparks of reasonable size.

Simulations with couplons of increasing length led to better-defined modes, of course at greater amplitudes (Stern et al., 1997). Under caffeine, the effects of which include increased CICR sensitivity (Herrmann-Frank et al., 1999), the number of channels activating in a spark would increase, leading to the better definition of modes.

A couplon simulation of the effects of increased CICR sensitivity is presented in Fig. 9. The calculations are carried out using the definitions of Stern et al. (1997) and the set of parameters listed in their Table 1. Half of the channels in the couplon are supposed to be Ca^{2+}-sensitive, gating among four states according to the diagram in A, where activation (C→O) and inactivation (O→I) are driven by Ca^{2+} binding to specific sites. The graphs illustrate the effect of increasing the sensitivity to activation by Ca^{2+}, represented in the model as an increase in k_o, the forward constant of the C→O transition. Shown is the distribution of maximum number of channels open simultaneously, in 10,000 discrete events occurring in multiple Monte Carlo realizations of the model. The distribution exhibits an ill-defined mode in the "reference" condition of lowest k_o (A). The mode shifts to higher numbers and increases its definition when k_o is doubled (B) or quadrupled (C). Additional effects, not illustrated, are an increase in the mean and mode of the distribution of event durations, and a shift and increase in definition of the mode in the amplitude distribution, similar to that in the number of open channels.

Through changes in a single parameter, the simulation therefore reproduces the observed effects of caffeine, with an important exception: it predicts an increase in amplitude, while no increase in average amplitude was observed in the present experiments (even for the corrected *g* distribution), and only a minor one was found in the study of González et al. (2000a). Reasons for the discrepancy include an increase in resting fluorescence (which directly reduces the normalized amplitude of the events) and partial depletion of Ca^{2+} (because a measurable increase in resting fluorescence probably reflects an increase in resting $[Ca^{2+}]$, hence a displacement of Ca^{2+} away from the sarcoplasmic reticulum).

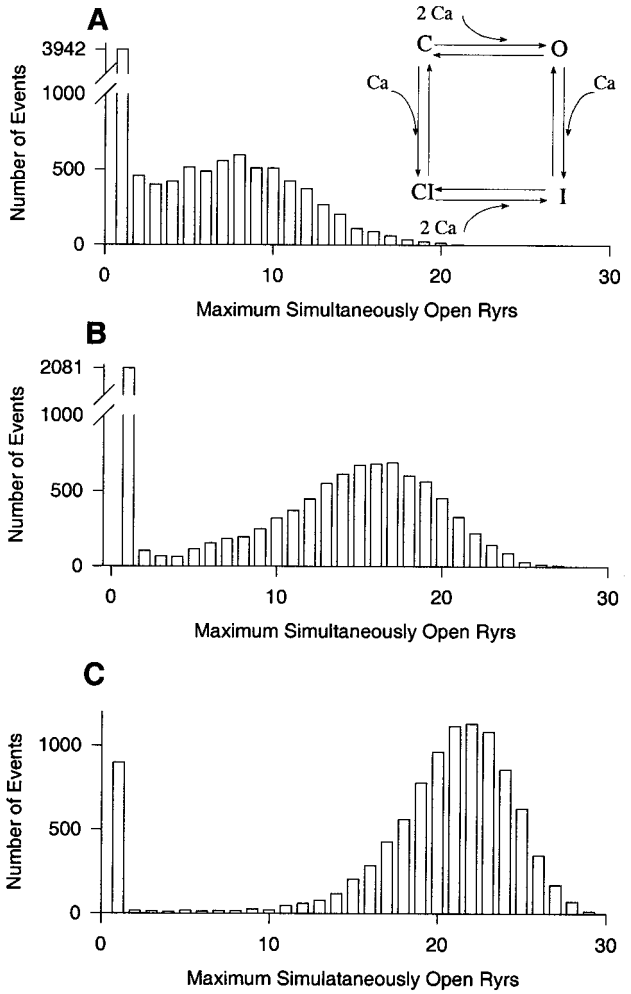

FIGURE 9 The couplon model generates sparks with modal distributions. Distribution of the maximum number of simultaneously open channels in discrete events (sparks) generated by a couplon with the structure and properties chosen by Stern et al. (1997). It consisted of 28 channels, 14 voltage-operated (*V*) and 14 gated by Ca^{2+} (*C*) according to the diagram in A, with states C (closed), O (open), I (inactivated), and CI (closed-inactivated). *V* channels were activated by voltage sensors according to the allosteric model of Ríos et al. (1993) and were Ca^{2+}-insensitive. The evolution of the model was computed by Monte Carlo simulation of a couplon held steadily at −70 mV, until 10,000 events were generated for each set of parameters. An event was accepted when it included opening of at least one *C* channel. The three distributions were generated changing the value of k_o, the forward rate constant of the activating transition (C→O), from 50 $\mu M^{-2}s^{-1}$ (*A*) to 100 $\mu M^{-2}s^{-1}$ (*B*) or 200 $\mu M^{-2}s^{-1}$ (*C*). Other parameters and their values are listed in Table 1 of Stern et al. (1997).

In spite of these reasonably successful simulations, the couplon model should not be regarded as a definitive resolution of spark mechanisms. It implements ad hoc a Ca^{2+}-dependent inactivation process that is inconsistent with the inactivation properties of release channels in bilayers (for assuming a dissociation constant of 10 μM for the inacti-

vation site). Additionally, it fails to produce the almost synchronous closure of channels demanded by the rapid termination of release in sparks (Lacampagne et al., 1999).

Average amplitude of Ca^{2+} sparks

As stated, the true amplitude of an individual spark is unknowable, because the location of the source is never determined. The present algorithm, however, provides statistical knowledge (the distribution g of amplitudes) and affords central measures: mode, median, or mean. It is interesting to compare such measures of the corrected distribution with those of the distribution of measured amplitudes (the amplitude histogram). The table shows that the mode of the distribution g is approximately 2.5 times greater than the average of the measured amplitudes (the other central measures of g, not listed, are close to the mode). Obviously, this ratio is somewhat variable, as it depends on the sensitivity of the detector and the threshold at which it is set, but is sufficiently well defined to provide a useful rule of thumb: when nothing is known regarding the position of a spark, its amplitude is likely to be underestimated two- to threefold, due to the uncertainty in location of the source relative to the scanning line. This is an important consideration, for instance, when using the amplitude of sparks as indication of the underlying currents and numbers of channels. Rather than the average amplitude (used, for instance, by Ríos et al., 1999), an adequate model should account for an amplitude 2 to 3 times greater.

APPENDIX A: AMPLITUDE HISTOGRAM OF A GAUSSIAN SPARK

The goal is to prove that the amplitude histogram of sparks in a confocal line scan image has the analytical form given by text Eq. 2 in a special case. The detected amplitude function $a(y,z)$, illustrated in Fig. 2 *A*, is defined as the amplitude with which a spark of full image amplitude a_{max} would be detected in a line scan if it originated at a position x,y,z and the scanned line was at $(x,0,0)$. The detected amplitude function is derived from an experimental spark $F(x, t)$ using the assumption that the spark is spherically symmetric. We will assume for simplicity that the imaging properties of the microscope (determining its PSF) are also symmetric. Under these hypotheses $a(y,z)$ is also symmetric. Specifically, it is a function $a(\rho)$ of the distance $\rho = \sqrt{(y^2 + z^2)}$ from the spark center to the scanned line, and the functional dependence, a, is the same as that of $F_{max}(x)$, derived from the spark $F(x, t)$ as described in the text.

Then, according to Eq. 1, when sparks of the same form are generated at random positions in the Z disks, at a rate of n per unit area of Z disk (during the time when the image is collected), the frequency of sparks in the image with detected amplitudes within an interval $(a, a + da)$ will be

$$f(a) = -n2\pi\rho(a)\frac{d\rho}{da} \tag{A1}$$

where $\rho(a)$ is the inverse of $a(\rho)$, existent because $a(\rho)$ is strictly monotonic.

The differential equation A1 can be integrated when $a(\rho)$ is Gaussian, that is:

$$a = \alpha e^{-\rho^2/2\sigma^2} \tag{A2}$$

Solving for ρ in Eq. A2 and substituting in Eq. A1 the result is

$$f(a) = n2\pi\frac{\sigma^2}{a} \tag{A3}$$

an expression valid for $a < \alpha = a_{max}$. This is the same as text Eq. 2.

APPENDIX B: LARGE SPARKS ARE CLOSER TO THE SCANNING LINE

The goal is to prove that a spark of greater measured amplitude is likely to have originated closer to the scanning line than one of lesser amplitude.

The only assumption needed is that the density $g(\alpha)$ of the distribution of full amplitudes has a mode, or, at least, decays beyond a certain value of α and eventually reaches 0.

Let a be the measured amplitude of a spark. The expected value $E_a(\rho)$ of the distance ρ of its source to the scanning line, can be calculated, and is proportional to

$$\int_0^{\rho_{max}} uG(a, u)du \tag{B1}$$

where the integration variable u takes the possible values of distance, between 0 and a maximum, ρ_{max}, corresponding to the distance at which the biggest possible spark is detected with amplitude a. $G(a,u)$ is the probability density of sparks such that the measured amplitude will be a when originating at distance u from the scanning line. If, for simplicity, we assume (the detected amplitude function of) sparks to be Gaussian, then Eq. A2 applies. Hence, α, the full amplitude of a spark detected with amplitude a at distance ρ, satisfies $\alpha = a\ \exp(k\rho^2)$, with $k = 1/2\sigma^2$. Therefore, $G(a,u) = g(a\ \exp(ku^2))$. Substituting in B1,

$$\int_0^{\rho_{max}} ug(ae^{ku^2})du \tag{B2}$$

Beyond a certain value of α, $g(\alpha)$ is assumed to decrease. Moreover, ρ_{max} is a decreasing function of the amplitude a; for both reasons, the integral (B2) will decrease with a, at least for a beyond a certain value. Therefore, the expected value of the distance from spark source and scanning line is a decreasing function of the measured spark amplitude, as hypothesized. (The derivation used a Gaussian shape for the detected amplitude function, but only as an example. This function determines a factor in the argument of g (in B2) whose specific form is irrelevant to the proof.)

This work was supported by grants from the National Institutes of Health (to E. R.), by intramural research programs of National Institutes of Health (to M. D. S and H. C.), and by a grant from National Institutes of Health (to N. S.). A. G. is the recipient of a Senior Fellowship from the American Heart Association of Metropolitan Chicago.

REFERENCES

Blatter, L. A., J. Hüser, and E. Ríos. 1997. Sarcoplasmic reticulum Ca^{2+} release flux underlying Ca^{2+} sparks in cardiac muscle. *Proc. Natl. Acad. Sci. USA.* 94:4176–4181.

Bridge, J. H., P. R. Ershler, and M. B. Cannell. 1999. Properties of Ca^{2+} sparks evoked by action potentials in mouse ventricular myocytes. *J. Physiol.* 518:469–478.

Brun, G., A. González, J. Rengifo, N. Shirokova and E. Ríos. 2000. Fast imaging in two dimensions resolves extensive sources of Ca^{2+} sparks in frog skeletal muscle. *J. Physiol.* 528:419–433.

Cannell, M. B., and C. Soeller. 1999. Mechanisms underlying calcium sparks in cardiac muscle. *J. Gen. Physiol.* 113:373–376.

Chen, T., and C. Miller. 1996. Nonequilibrium gating and voltage dependence of the ClC-0 Cl^- channel. *J. Gen. Physiol.* 108:237–250.

Cheng, H., W. J. Lederer, and M. B. Cannell. 1993. Calcium sparks: elementary events underlying excitation-contraction coupling in heart muscle. *Science.* 262:740–744.

Cheng, H., L. S. Song, N. Shirokova, A. González, E. G. Lakatta, E. Ríos, and M. D. Stern. 1999. Amplitude distribution of calcium sparks in confocal images: theory and studies with an automatic detection method. *Biophys. J.* 76:606–617.

Colquhoun, D., and A. G. Hawkes. 1995. The principles of the stochastic interpretation of ion-channel mechanisms. *In* Single Channel Recording, chapter 18, second edition. B. Sakmann, and E. Neher, editors. Plenum Press, New York. 397–482.

Endo, M., M. Tanaka, and Y. Ogawa. 1970. Calcium induced release of calcium from the sarcoplasmic reticulum of skinned skeletal muscle fibres. *Nature.* 228:34–36.

Franzini-Armstrong, C., and A. O. Jorgensen. 1994. Structure and development of E-C coupling units in skeletal muscle. *Annu. Rev. Physiol.* 56:509–534.

González, A., W. G. Kirsch, N. Shirokova, G. Pizarro, M. D. Stern, and E. Ríos. 2000a. The spark and its ember: separately gated local components of Ca^{2+} release in skeletal muscle. *J. Gen. Physiol.* 115:139–158.

González, A., W. G. Kirsch, N. Shirokova, G. Pizarro, G. Brum, I. N. Pessah, M. D. Stern, H. Cheng, and E. Ríos. 2000b. Involvement of multiple intracellular release channels in calcium sparks of skeletal muscle. *Proc. Natl. Acad. Sci. USA.* 97:4380–4385.

Gration, K. A., J. J. Lambert, R. L. Ramsey, R. P. Rand, and P. N. Usherwood. 1982. Closure of membrane channels gated by glutamate receptors may be a two-step process. *Nature.* 295:599–603.

Herrmann-Frank, A., H.-C. Lüttgau, and D. G. Stephenson. 1999. Caffeine and excitation-contraction coupling in skeletal muscle: a stimulating story. *J. Mus. Res. Cell Motil.* 20:223–237.

Izu, L. T., W. G. Wier, and C. W. Balke. 1998. Theoretical analysis of the Ca^{2+} spark amplitude distribution. *Biophys. J.* 75:1144–1162.

Jiang, Y. H., M. G. Klein, and M. F. Schneider. 1999. Numerical simulation of Ca^{2+} "sparks" in skeletal muscle. *Biophys. J.* 77:2333–2357.

Kettlun, C., A. González, W. Nonner, E. Ríos, and M. Fill. 2000. Ryanodine receptor unitary Ca^{2+} current is greater in frog skeletal muscle than in mammalian heart. *Biophys. J.* 78:437A (abstr.).

Klein, M. G., H. Cheng, L. F. Santana, Y. H. Jiang, W. J. Lederer, and M. F. Schneider. 1996. Two mechanisms of quantized calcium release in skeletal muscle. *Nature.* 379:455–458.

Lacampagne, A., C. W. Ward, M. G. Klein, and M. F. Schneider. 1999. Time course of individual voltage-activated Ca^{2+} sparks recorded at ultra-high time resolution in frog skeletal muscle. *J. Gen. Physiol.* 113:187–198.

López-López, J. R., P. S. Shacklock, C. W. Balke, and W. G. Wier. 1995. Local calcium transients triggered by single L-type calcium channel currents in cardiac cells. *Science.* 268:1042–1045.

Nelson, M. T., H. Cheng, M. Rubart, L. F. Santana, A. D. Bonev, H. J. Knot, and W. J. Lederer. 1995. Relaxation of arterial smooth muscle by calcium sparks. *Science.* 270:633–637.

Park, S., and R. Schowengerdt. 1983. Image reconstruction by parametric cubic convolution. *Comp. Vis. Graph. Image Process.* 23:256–265.

Pratusevich, V. R., and C. W. Balke. 1996. Factors shaping the confocal image of the calcium spark in cardiac muscle cells. *Biophys. J.* 71: 2942–2957.

Reif, F. 1962. Fundamentals of Statistical and Thermal Physics. McGraw-Hill, New York. 42.

Ríos, E., M. Karhanek, J. Ma, and A. González. 1993. An allosteric model of the molecular interactions of excitation-contraction coupling in skeletal muscle. *J. Gen. Physiol.* 102:449–482.

Ríos, E., M. D. Stern, A. González, G. Pizarro, and N. Shirokova. 1999. Calcium release flux underlying Ca^{2+} sparks of frog skeletal muscle. *J. Gen. Physiol.* 114:31–48.

Schneggenburger, R., and P. Ascher. 1997. Coupling of permeation and gating in an NMDA-channel pore mutant. *Neuron.* 18:167–77.

Schneider, M. F. 1999. Ca^{2+} sparks in frog skeletal muscle: generation by one, some, or many SR Ca^{2+} release channels? *J. Gen. Physiol.* 113: 365–72.

Sham, J. S., L. S. Song, Y. Chen, L. H. Deng, M. D. Stern, E. G. Lakatta, and H. Cheng. 1998. Termination of Ca^{2+} release by a local inactivation of ryanodine receptors in cardiac myocytes. *Proc. Natl. Acad. Sci. USA.* 95:15096–15101.

Shirokova, N., and E. Ríos. 1997. Small event Ca^{2+} release: a probable precursor of Ca^{2+} sparks in frog skeletal muscle. *J. Physiol. (Lond.).* 502:3–11.

Shirokova., N., A. González, W. G. Kirsch, E. Ríos, G. Pizarro, M. D. Stern, and H. Cheng. 1999. Calcium sparks: release packets of uncertain origin and fundamental role. *J. Gen. Physiol.* 113:377–384.

Smith, G. D., J. E. Keizer, M. D. Stern, W. J. Lederer, and H. Cheng. 1998. A simple numerical model of calcium spark formation and detection in cardiac myocytes. *Biophys. J.* 75:15–32.

Stern, M. D., G. Pizarro, and E. Ríos. 1997. Local control model of excitation-contraction coupling in skeletal muscle. *J. Gen. Physiol.* 110:415–440.

Tripathy, A., and G. Meissner. 1996. Sarcoplasmic reticulum lumenal Ca^{2+} has access to cytosolic activation and inactivation sites of skeletal muscle Ca^{2+} release channel. *Biophys. J.* 70:2600–2615.

Tsugorka, A., E. Ríos, and L. A. Blatter. 1995. Imaging elementary events of calcium release in skeletal muscle cells. *Science.* 269:1723–1726.

Wang, S. Q., L. S. Song, L. Xu, G. Meissner, E. G. Lakatta, E. Ríos, M. D. Stern, and H. Cheng. 2000. Ca-driven irreversible gating of single ryuanodine receptors reproduces the stereotyped duration of Ca sparks. *Biophys. J.* 78:437A (abstr.).

Xu, L., and G. Meissner. 1998. Regulation of cardiac muscle Ca^{2+} release channel by sarcoplasmic reticulum lumenal Ca^{2+}. *Biophys. J.* 75: 2302–2312.